

Article

Wireless Data Acquisition System with Feedback Function

Anatoliy Manukovsky, Aigerim Sagyndyk * , Aleksandr Kislov, Olzhas Talipov and Alexey Manukovsky

Electrical Engineering and Automation Department, Toraighyrov University, Lomov Str. 64, Pavlodar 140008, Kazakhstan; manukovskii.a@teachers.tou.edu.kz (A.M.); kislov.a@teachers.tou.edu.kz (A.K.); talipov.o@teachers.tou.edu.kz (O.T.); manukovskiy.a@teachers.tou.edu.kz (A.M.)

* Correspondence: sagyndyk.a@teachers.tou.edu.kz; Tel.: +7-701-242-7295

Abstract: When operating solar–wind power plants (SWPPs) located in populated areas, cases of premature failure of expensive batteries and other power equipment often occur. The purpose of this study is to develop a wireless data acquisition system (DAS) for the operation of an SWPP with a feedback function to prevent material damage from the failure of power equipment and to increase the efficiency of natural energy use. The principles of constructing a DAS, free from some of the disadvantages of analogues, are described in this paper. Intelligent wireless current and voltage sensors and a device for receiving and recording data with an additional feedback function have been developed, providing real-time feedback when the measured parameters go outside the norm. Measurement data are displayed on the laptop screen and alphanumeric display and stored on the hard drive along with timestamps and current event messages. An example of using a reverse communication channel to implement the functions of backup battery protection and to switch SWPP loads is described. The principles and methods proposed in this article are suitable for constructing systems for remote measurements of any physical quantities; therefore, the scope of application of the described system can be significantly expanded.

Keywords: data acquisition system; wireless sensor; microcontroller; radio module; infrared receiver



Citation: Manukovsky, A.; Sagyndyk, A.; Kislov, A.; Talipov, O.; Manukovsky, A. Wireless Data Acquisition System with Feedback Function. *Appl. Sci.* **2024**, *14*, 5553. <https://doi.org/10.3390/app14135553>

Academic Editor: Alessandro Lo Schiavo

Received: 30 May 2024

Revised: 20 June 2024

Accepted: 21 June 2024

Published: 26 June 2024



Copyright: © 2024 by the authors. Licensee MDPI, Basel, Switzerland. This article is an open access article distributed under the terms and conditions of the Creative Commons Attribution (CC BY) license (<https://creativecommons.org/licenses/by/4.0/>).

1. Introduction

The hybrid utilization of photovoltaic (PV) cells and wind turbines (WTs) is one of the most promising technologies among renewable energy sources for satisfying the load demand because the two have complementary energy generation profiles [1–3]. When operating solar–wind power plants (SWPPs) located in populated areas, cases of premature failure of expensive batteries and other power equipment quite often occur [1–6]. Most often, this failure occurs due to the use of algorithms for controlling the operation of solar power plants that do not take into account the peculiarities of their joint operation with existing urban or rural power supply networks, and less often due to a malfunction or incorrect configuration of solar panel or wind generator controllers. Studies [1,6] also note that any system is prone to present faults not only due to incorrect initial installation procedures, but also due to the effects of wear and the aging of components during operation.

Thanks to the opportunity to observe for a long time the operation of low-power SWPPs of two universities in the city of Pavlodar, the authors came to the conclusion that the control algorithms for the operation of Green Energy power plants (GEPPs), often hardwired into standard power equipment, are more suitable for cases of GEPP operation in remote areas, for example, on distant pastures or in mobile homes. Under the conditions of joint work of GEPPs with existing utility power supply networks, such algorithms do not provide satisfactory technical and economic results in relation to their operation and even lead to losses due to accelerated wear of the main power components. This is not surprising—after all, in the two above-mentioned location cases, diametrically opposed requirements are placed on the GEPP. In the first case, the GEPP is subject to a categorical requirement to ensure that consumers are powered by Green Energy sources and batteries

for as long as possible. The battery depth of discharge (DOD) is close to 100% and cannot be significantly limited by controller settings. The service life of even the best modern batteries is reduced several times in this case. The family of typical DOD curves for CHALLENGER G12-200 (Ritar International Group, Hengyang, Hunan, China) batteries is shown in Appendix A. In the case of a GEPP located in a populated area, the depth of discharge of the batteries can be limited without harm to consumers by transferring them to power from the utility network upon reaching a DOD level acceptable in terms of service life. In addition, if there is an excess of wind and/or solar energy, additional electrical loads can be connected to GEPPs located near inhabited buildings, as described further in Section 2, and thus increase the efficiency of using free natural energy. It is obvious that standard GEPP equipment and the algorithms embedded in it do not allow us to implement the proposed improvements in low-power GEPPs located near inhabited buildings, even taking into account the possibility of custom settings of standard controllers. This requires the development of additional hardware and software. Criteria for setting up these additional tools can only be developed based on a detailed analysis of monitoring data for the operation of a specific GEPP.

The purpose of this study is to develop a wireless data acquisition system (DAS) for the operation of low-power solar power plants (up to 10–20 kW) with a feedback function to prevent material damage from the failure of power equipment and to improve the efficiency of natural energy use.

The set goals can be achieved as follows:

- Due to the timely prevention of the consequences of emergency conditions by organizing an automatic feedback response of the data collection system to the incorrect operation of the standard equipment of the SWPP;
- By automatically switching, using feedback, part of the SWPP loads from power from the public electrical network to power from natural energy when there is an excess of it and vice versa when there is a lack of it;
- By identifying abnormal and ineffective operating modes of equipment by analyzing the results of monitoring the main parameters of the functioning of the SWPP.

An analysis of the monitoring data accumulated over a long period of time will make it possible in the future to further improve the equipment and algorithms for controlling the functioning of the SWPP and to tailor them to work together with existing utility power supply networks. The need to develop a data collection system for monitoring the operation of “Green Energy” power plants has been repeatedly substantiated previously, for example, in [7–27].

Thus, further research in the field of improving DASs for GEPPs is currently necessary and is an urgent task. For these reasons, great efforts are being made in the development of methods for monitoring the operation of “Green Energy” power plants by the scientific community. The results of the current study can serve as the basis for improving the algorithms for the operation of low-power “Green Energy” power plants located in populated areas.

The following data transmission channels are used in GEPP operation monitoring systems:

- (1) Wired channels, which have two subcategories:
 - (a) Coaxial cables or twisted pairs [9–12].
 - (b) Fiber optic cables [13–15].
- (2) Power line communication (PLC) [16,17].
- (3) Wireless connection [18–27].

Wired channels provide high-speed transmission of large amounts of data, but due to the high cost of cable products and the complexity of installation, they are not suitable for building low-power GEPP monitoring systems, in which high transmission speeds are usually not required, and data volumes are in the tens or hundreds of bytes. The limited applicability of PLC technology for monitoring GEPP operation is proven, in particular, by recent studies [28], which confirm that the level of noise and interference in power

line communication (PLC) is much higher than in any other communication network. Using a wired connection on GEPPs is not always acceptable due to the additional wiring required. At the same time, wireless networks have evolved significantly over the past few years, providing low-cost and energy-efficient solutions with reliable data collection and sufficient real-time performance, ensuring lossless data transmission to the final destination. Therefore, monitoring system developers are increasingly choosing wireless solutions. In [18–20], communication is based on the GSM network. In particular, they use the short message service (SMS). However, it should be noted that this channel in places with unstable communication is not always capable of providing data transmission in real time, since in the GSM network, voice communication has the highest priority, followed by data service, and SMS transmission has the lowest priority [29]. In [21,22], a wireless technology based on ZigBee is proposed to provide online monitoring systems for photovoltaic power plants. However, to build a ZigBee network, microcontrollers with a flash memory capacity of 128 kB or more are required, as well as the purchase of licensed software in the form of the so-called ZigBee stack [30], which makes their use for building low-power DASs for GEPPs economically unfeasible. The widespread availability of inexpensive energy-saving radio modules (ESRMs) with convenient interfaces for interfacing with microcontrollers (MCUs) gives developers of wireless data acquisition systems new opportunities, and in simple, unbranched low-power GEPP networks, their use may well compete with ZigBee technology. In [23] and some others, data are sent to the user's PC in the form of a Wi-Fi signal, which limits the range compared to ESRMs in places far from routers. For instance, the range of the popular and inexpensive ESRM type HC-12 with a convenient UART interface is 1000 m [31]. In more recent works [24–26], the authors adopted Internet of Things (IoT) technology for solar energy monitoring. Despite the fact that IoT is a modern and seemingly perfect solution for monitoring solar power plants, this technology may be at risk of cyberattacks and operational failures [32–34].

In the block diagram in Figure 1, the authors tried to summarize the currently used typical solutions for building wireless data acquisition systems (DASs) for GEPPs with a power of up to 10–20 kW. In Figure 1, the red lines indicate wires connecting remote DAS nodes. The abbreviations in the diagram are deciphered as follows: SVS—supply voltage shaper, AS—analog sensor, VA—voltage amplifier, DS—digital sensor, ADC—analog to digital converter, MCU—microcontroller unit, DSD—data display, recording, and storage unit (most often a laptop, sometimes LCD indicator and microSD card), and TX—data transmitter (an ESRM can be used, but more often a GSM module, a Wi-Fi module, a Bluetooth module, or IoT is used).

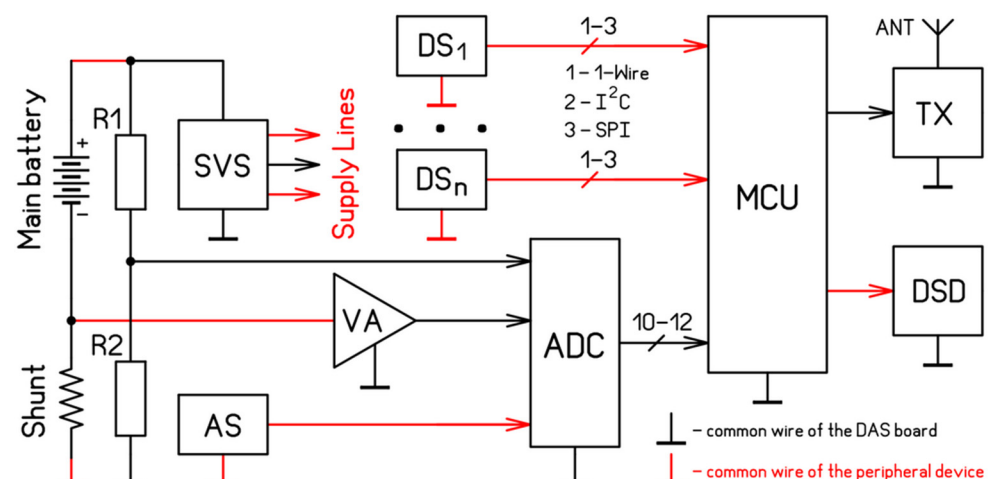


Figure 1. Block diagram of typical wireless data acquisition system.

The disadvantage of the standard circuit is the galvanic connection between all components of the DAS and GEPP via common wire (Gnd). This does not allow us, in particular, to measure the voltage of each of several series-connected batteries in the described system. In low-power GEPPs with a nominal main battery voltage of, for instance, 48 V, it is typical to use sections of four 12 V batteries connected in series. Since over time, the parameters of power batteries vary more and more, a case may occur when the total battery voltage is normal, while individual batteries will be overdischarged, and others will be overcharged. This can cause the electrolyte to “boil over” and sulfation of the plates, followed by an avalanche-like increase in the internal resistance and voltage of the battery, its overheating, and a decrease in the ability of the entire main battery to accept and release charge. Therefore, monitoring the voltage of each battery is absolutely necessary.

In a typical design, the supply voltages for all of the central and peripheral DAS modules are generated from the main battery voltage using a supply voltage shaper (SVS). The lines marked in red feed sensors farther away from the main DAS module and are longer, as are the lines from the shunt and from the main battery, and the lines from the central DAS module to the DSD module. The lines connecting the common peripheral wires to the central DAS module are also longer. The signal lines of the sensors are also longer, often consisting of two or three conductors, depending on the type of interface. The total number of lines for connecting one digital sensor can reach 5. For complete diagnostics, in addition to voltage, it is also necessary to measure the temperature of each battery. Temperature sensors must have thermal contact with each battery. It turns out that the DAS, being wireless, actually has the form of a device to which a large number of long wires are connected, even if a modern specialized DAQ card is used to connect sensors, such as National Instrument USB-6009 (Austin, TX, USA) with 8 inputs and a 14-bit multisystem I/O.

In addition, regarding the reasons given in Section 1, when using IoT, Wi-Fi, and GSM technologies, failures and interruptions in data transmission are possible.

Among the disadvantages of all of the DASs considered is the absence in their composition of at least the simplest means of diagnosing the serviceability of their components. It is also unknown how the system will behave and what will be recorded in the DAS monitoring protocol discussed in Section 1 if the cables of one or more sensors fail or break.

Many of the data collection systems discussed in this review allow you to collect and process data in real time, as well as exchange data with a central control system that uses artificial intelligence to speed up the response to events. However, small GEPPs with a power of up to 10–20 kW, as a rule, are not connected to the central control system, and the recorded data, due to the lack of full-time employees, are processed with a time delay of several days or even weeks. This problem is highlighted particularly clearly in DAS variants that record data on SD cards and transmit them via the Bluetooth interface [27]. Such a delay is acceptable provided that all GEPP equipment is in good working order and is set up correctly after commissioning. If at least one of these conditions is not met, then equipment failure during automatic monitoring without constant or at least regular monitoring by people can be prevented only by adding to the DAS the function of automatically responding to problems and abnormal conditions.

2.2. Improved DAS Design Concept for Low-Power GEPPs

The concept of building a wireless DAS option, free from the gaps and weaknesses noted in Sections 1 and 2.1, is explained by the block diagram shown in Figure 2.

The red rectangles in the upper left quadrant of the diagram indicate wireless smart sensors, each of which contains a primary measuring transducer PMT, a radio transmitter TX with an antenna, an infrared receiver IRR, and a microcontroller not shown in the diagram located in one housing. In the practical implementation of sensors, all of the listed modules are selected from among widely available products that have low-power consumption modes, which makes it possible to power them from small-capacity batteries. The sensors differ from each other only in the PMT module, which is selected

depending on the type of physical parameter X being measured. Many modern digital sensors can convert two physical parameters simultaneously into a digital signal. In the diagram, they are indicated by the letters X and Y . For example, a BMP280-type sensor can output the measurement results of both atmospheric pressure and temperature to the microcontroller [35]. For the purpose of galvanic isolation, each sensor is powered by a separate GB. This gives us freedom to choose the placement of sensors and the ability to connect them to GEPP equipment at different potentials in relation to the common wire. In particular, this approach makes it possible to easily organize the measurement of the voltage of each individual battery in a chain of series-connected power batteries PA1...PA4. For this purpose, in the left column of the sensors shown in Figure 2 (VCS #1, VCS#2), it is enough to select specialized voltage and current sensors (VCSs) as the PMT. Since the current strength in batteries PA1...PA4 is the same, the current measurement pin is connected only to VCS #1, and for the remaining sensors VCS #2...VCS #4, it is not used. Choosing popular digital temperature sensors (for example, DS18B20) as the PMT makes it easy to perform the temperature measurement of each power battery separately and, in general, in any other places of the GEPP. In discrete value sensors of the “0/1” type, it is possible to forgo the purchase of a PMT by using microcontroller ports with level matching circuits and protection against overvoltage and impulse noise for its implementation.

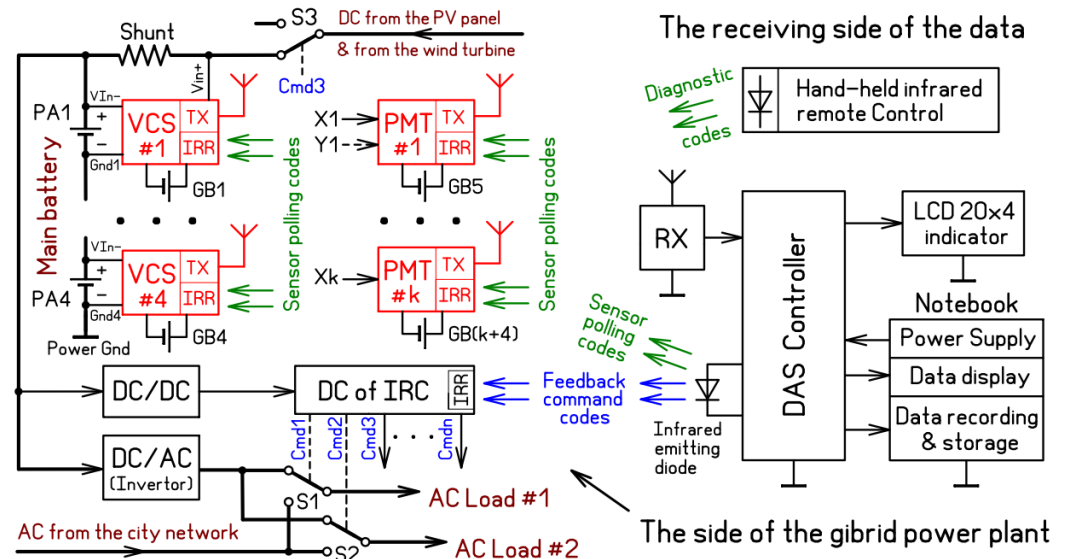


Figure 2. Wireless DAS block diagram for low-power GEPPs.

Most of the time, all wireless sensor modules, except the low-power IRR, are in energy-saving sleep mode. The waking up and polling of sensors are carried out by the DAS controller one by one via the infrared channel, so these processes cannot be disrupted by external influences via the radio channel. The sensors only transmit data using simple ESRMs, so the resistance of the sensors to external influences over the radio channel is higher than when ZigBee transceiver modules are used for this purpose, and the security of the entire system is higher than when using the Internet.

The reception of data packets, verification of reliability, and decoding of sensor signals are carried out by the DAS controller from each sensor in turn using a simple RX receiving radio module, which does not have built-in functions for calculating the checksum and confirming reception. The software of the DAS controller ensures that information received from the sensors is displayed with time stamps on the laptop monitor screen and recorded on the hard drive. Unlike analogues, a significant part of the received information is also displayed on a 4-line LCD indicator, which makes it possible not to keep the laptop screen constantly on and thus save the resource of its battery, which is used to reserve power for the DAS receiving part during power outages. Unlike analogues, in the proposed DAS concept, the received data are not only recorded, but also analyzed in real time, and if their

values deviate from the norm, the DAS controller immediately issues a system response to these deviations in the form of IR commands. Commands are decrypted on the power equipment side using an infrared command decoder (DC IRC), powered from the main battery through a step-down DC/DC converter. After decoding, the commands act on the GEPP power equipment through executive units (EUs).

Let us consider the behavior of the proposed system in various situations. At a normal voltage of each battery, switch S3 of the main battery charging circuit is closed, and the standard Load1 is connected to the output of the GEPP inverter at the right time. If there is a dangerous excess voltage of at least one battery, two options for automatic system response are possible. In the most straightforward version, the system's reaction could be to issue the command Cmd3 to turn off the main battery charging circuit with switch S3. However, this solution is not the most optimal, as it leads to the underutilization of natural energy. The best option in this case is to issue commands to switch the additional AC Load #2 from utility power to GEPP power. A load of this nature (or even several of them) can always be found and connected to low-power GEPPs, located, as a rule, close to inhabited buildings. This could be, for example, ventilation and lighting installations, advertising structures, etc. An increase in the GEPP load current will cause a decrease in the voltage of each battery, but due to the presence of hysteresis in the subroutine for responding to voltage changes, issuing commands to turn off the loads will not occur until the voltage of at least one of the power batteries PA1...PA4 reaches the lower permissible threshold. Therefore, all "extra" natural energy will be effectively used. To prevent flicker operation of switches S1 and S2, the DAS controller must be set to the correct lower and upper thresholds for issuing and removing commands Cmd1–Cmd3 and the corresponding time delays.

If there is a dangerous drop in voltage of at least one battery, the DAS controller switches the loads to power from the utility network with a time delay, preventing battery failure. The ability to transmit a large number of feedback commands provides great opportunities not only to prevent the failure of GEPP equipment, but also to implement various promising options for optimizing the process of converting natural energy into electrical energy.

The proprietary software for the sensors and DAS controller developed by the authors made it possible to ensure that there are no disruptions to the monitoring process of the remaining sensors when any sensors are turned off during operation, as well as "hot" automatic activation of the sensors registered in the system. The number of sensors in the system is limited almost only by the maximum permissible increase in the sensor polling cycle time. For example, with an interval between polling pulses of 0.5 s and a number of sensors of 32, the cycle time will be 16 s. The minimum interval limitation of 0.5 s is due to the finite amount of time it takes for the wireless sensor components to wake up from sleep mode.

Unlike most DAS construction concepts analyzed in Section 1, the proposed concept allows one to connect a large number of sensors to the system and place them in any convenient GEPP locations without increasing the number and length of connecting wires, that is, to implement a truly wireless DAS.

The proposed system also implements the function of online remote diagnostics of sensor status, which is not available in analogues, without connecting additional wires using requests submitted from a hand-held IR remote control in pauses between polling pulses, as shown in Figure 2. Diagnostic requests are received by the infrared receivers (IRRs) included in each smart sensor. The diagnostic process is described in detail in Appendix B and, in part, in Section 2.3.

The team of authors designed, manufactured, and tested a full-scale model of the proposed DAS, containing part of its components, the minimum required to begin the practical use of DAS. The results of testing the model at the SWPP of Toraighyrov University in the city of Pavlodar confirmed the correctness of the ideas embedded in the proposed concept and proved the performance of the technical solutions and software used for its implementation.

Details of the implementation of the proposed concept and the results of full-scale tests of the DAS prototype are described in the following sections.

2.3. Obtaining Initial Information about Current and Voltage

To ensure the functionality of the monitoring system, at a minimum, information about the current and voltage in the power circuits is required [7,36]. Currently, there is no doubt that measurements and data transfer must be carried out in digital form. A typical way to measure and digitize constant voltage today is to use analog-to-digital converters (ADCs) with the averages of multiple samples to reduce amplitude jitter. For this purpose, as a rule, ADCs that are part of modern microcontrollers (MCUs) are most often used. However, the reference voltage in such ADCs usually does not exceed 5 V, and to bring higher voltage levels in the power circuits of the SWPP to the input voltage range of the built-in ADC, it is necessary to use resistive voltage dividers, as shown in Figure 1. When measuring current to measure small voltages on shunts or Hall sensors, it is impossible to do so without additional direct current amplifiers, which are subject to zero drift at their outputs and require a bipolar power supply [37]. Along with a decrease in resolution and accuracy, all this complicates the sensor design and forces the use of more expensive MCUs with 12-bit ADCs. The approach to the selection of equipment for measuring direct current and voltage is radically changed by the appearance on the general market [38] of inexpensive digital sensors in an integrated design, which make it possible to comprehensively solve all of the above problems.

To obtain primary information about current and voltage directly in digital form, the most suitable sensors in our case were the INA219 sensors, allowing for the simultaneous measurement of not only voltage, but also the strength and power of the direct current. A block diagram of the INA219 current and voltage sensors is shown in Figure 3. These sensors already contain inside the crystal [39] a measurement mode switch (current–voltage), a pre-amplifier, and a built-in 12-bit ADC, which provides much higher metrological and speed parameters than the 10-bit ADC of most widely used microcontrollers. In addition, they are very compact and economical, consuming no more than 1 mW in the power supply circuit. Using one such sensor, you can simultaneously measure voltage up to 26 V, current up to 3.2 A, and power up to 83 W with high accuracy. To expand the current and power measurement limits, an external shunt is used.

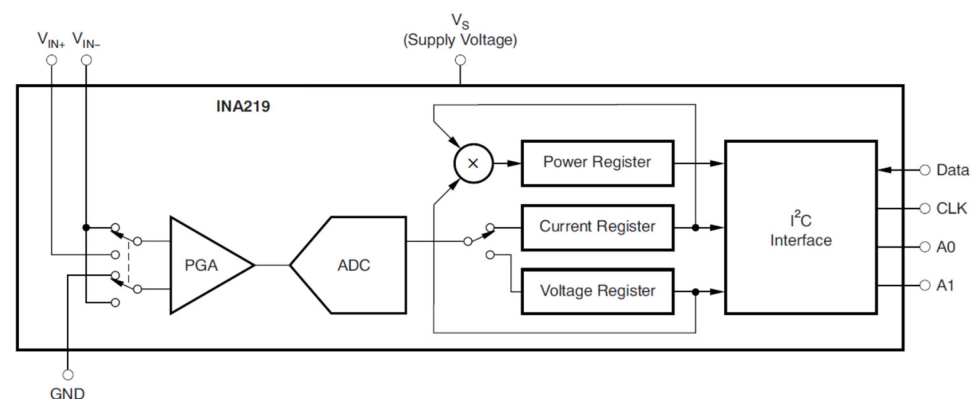
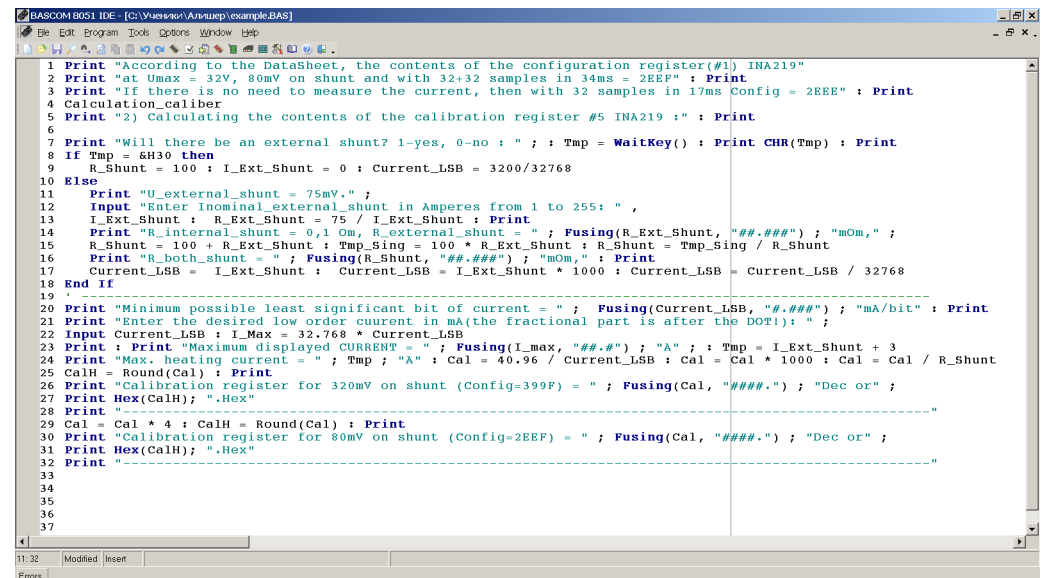


Figure 3. Block diagram of INA219 current and voltage sensors.

Current measurement is carried out using a 0.1 Ohm resistor (shunt) with an accuracy of 1% (inputs V_{in+} and V_{in-}). The microcircuit, by averaging a given number of ADC samples, measures the voltage at the terminals connecting the voltage and the voltage drop across the shunt, and then, according to the laws of electrical engineering, calculates the current and power and enters them into its internal registers. The contents of the registers can be read from the microcircuit via the I2C interface in a time of about 1 ms. Calculation of the contents of the INA219 registers for sensors intended for installation on the batteries of the SWPP of Toraighyrov University (ToU) was carried out in the BasCom-

AVR environment using a program compiled on the basis of the methodology from the datasheet of the INA219 module. A fragment of the program is shown in Figure 4. A more detailed description of the calculation algorithm included in the program is provided in Appendix C.



```

1 Print "According to the DataSheet, the contents of the configuration register (#1) INA219"
2 Print "at Umax = 32V, 80mV on shunt and with 32+32 samples in 34ms = 2EEF" : Print
3 Print "If there is no need to measure the current, then with 32 samples in 17ms Config = 2EEE" : Print
4 Calculation_caliber
5 Print "2) Calculating the contents of the calibration register #5 INA219 : " : Print
6
7 Print "Will there be an external shunt? 1=yes, 0=no : " ; Tmp = WaitKey() : Print CHR(Tmp) : Print
8 If Tmp = &H30 then
9   R_Shunt = 100 : I_Ext_Shunt = 0 : Current_LSB = 3200/32768
10 Else
11   Print "U_external_shunt = 75mV." ;
12   Input "Enter Inominal_external_shunt in Amperes from 1 to 255: " ,
13   I_Ext_Shunt : R_Ext_Shunt = 75 / I_Ext_Shunt : Print
14   Print "R_internal_shunt = 0,1 Ohm, R_external_shunt = " ; Fusing(R_Ext_Shunt, "###.##") ; "mOhm," ;
15   R_Shunt = 100 + R_Ext_Shunt : Tmp_Sing = 100 * R_Ext_Shunt : R_Shunt = Tmp_Sing / R_Shunt
16   Print "R_both_shunt = " ; Fusing(R_Shunt, "###.##") ; "mOhm," : Print
17   Current_LSB = I_Ext_Shunt : Current_LSB = I_Ext_Shunt * 1000 : Current_LSB = Current_LSB / 32768
18 End If
19
20 Print "Minimum possible least significant bit of current = " ; Fusing(Current_LSB, "###.##") ; "mA/bit" : Print
21 Print "Enter the desired low order current in mA(the fractional part is after the DOT!)" :
22 Input Current_LSB : I_Max = 32.768 * Current_LSB
23 Print : Print "Maximum displayed CURRENT = " ; Fusing(I_Max, "###.##") ; "A" ; : Tmp = I_Ext_Shunt + 3
24 Print "Max. heating current = " ; Tmp ; "A" : Cal = 40.96 / Current_LSB : Cal = Cal * 1000 : Cal = Cal / R_Shunt
25 CalH = Round(Cal) : Print
26 Print "Calibration register for 320mV on shunt (Config=399F) = " ; Fusing(Cal, "###.##") ; "Dec or" ;
27 Print Hex(CalH) ; ".Hex"
28 Print "-----"
29 Cal = Cal * 4 : CalH = Round(Cal) : Print
30 Print "Calibration register for 80mV on shunt (Config=2EEF) = " ; Fusing(Cal, "###.##") ; "Dec or" ;
31 Print Hex(CalH) ; ".Hex"
32 Print "-----"
33
34
35
36
37

```

Figure 4. A fragment of the program for calculating the contents of INA219 registers.

As a result of the calculation, for sensors measuring current with a shunt of 15 A, 75 mV, the values of the register Config = 2EEF (Hex) were obtained (averaging from 32 + 32 ADC samples for 34 ms), and for the register, Calibr = 8664. For voltage-only sensors, Config = 2EEE (average of 32 ADC samples in 17 ms; ADC does not waste time measuring current) and Calibr = 0000. The selected sensor settings provide a maximum displayed current of 32,8 A without register overflow and no jitter between repeated measurements. In order to avoid damage to the contents of the registers at the moment the power is turned on, the obtained calculated values are entered by the microcontroller into the sensor registers each time the control program is started.

2.4. Selecting Components for a Smart Wireless Sensor

The ability to configure the number of averaged ADC samples in the INA219 in combination with the output of the result in digital form allows you, in order to control the measurement process, to use an inexpensive MCU without an ADC with a program memory of 2 kB, for example, Attiny2313A from company Atmel (San Jose, CA, USA). The Attiny2313A MCU, for which a block diagram of the Attiny2313A microcontroller is shown in Figure 5, was chosen by the authors because of its ability to operate when the supply voltage drops down to 1.8 V and because of its low current consumption. Even at a clock frequency of 4 MHz, its current consumption at a supply voltage of 3.3 V does not exceed 2 mA [40].

For similar reasons, to build a wireless sensor, the authors used an infrared receiver TSOP31236 from Vishay (Dallas, TX, USA), capable of accurately receiving IR code messages at a distance of up to 24 m even when the supply voltage is reduced to 2.5 V [41]. A block diagram of the TSOP31236 infrared receiver is shown Figure 6.

To transmit measured current and voltage values via radio, the authors used the JDY-40 radio module, shown in Figure 7.

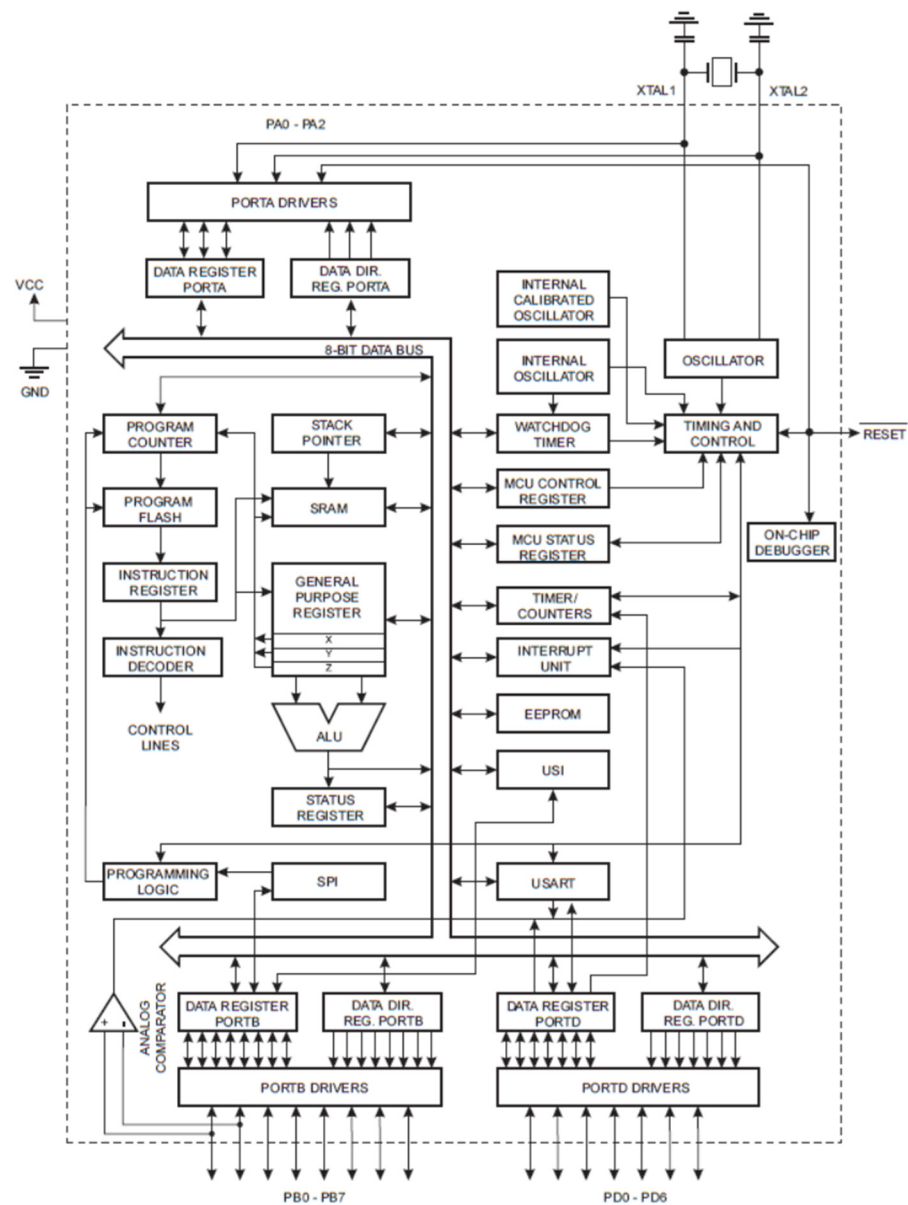


Figure 5. Block diagram of Attiny2313A microcontroller.

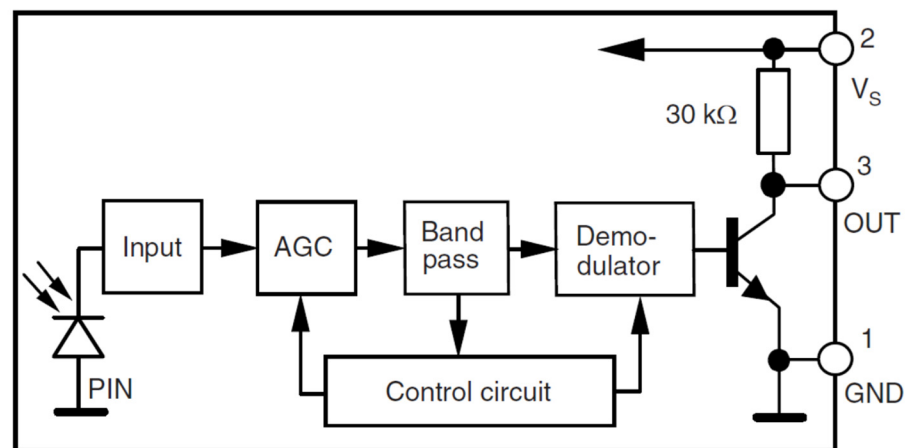


Figure 6. Block diagram of TSOP31236 infrared receiver.

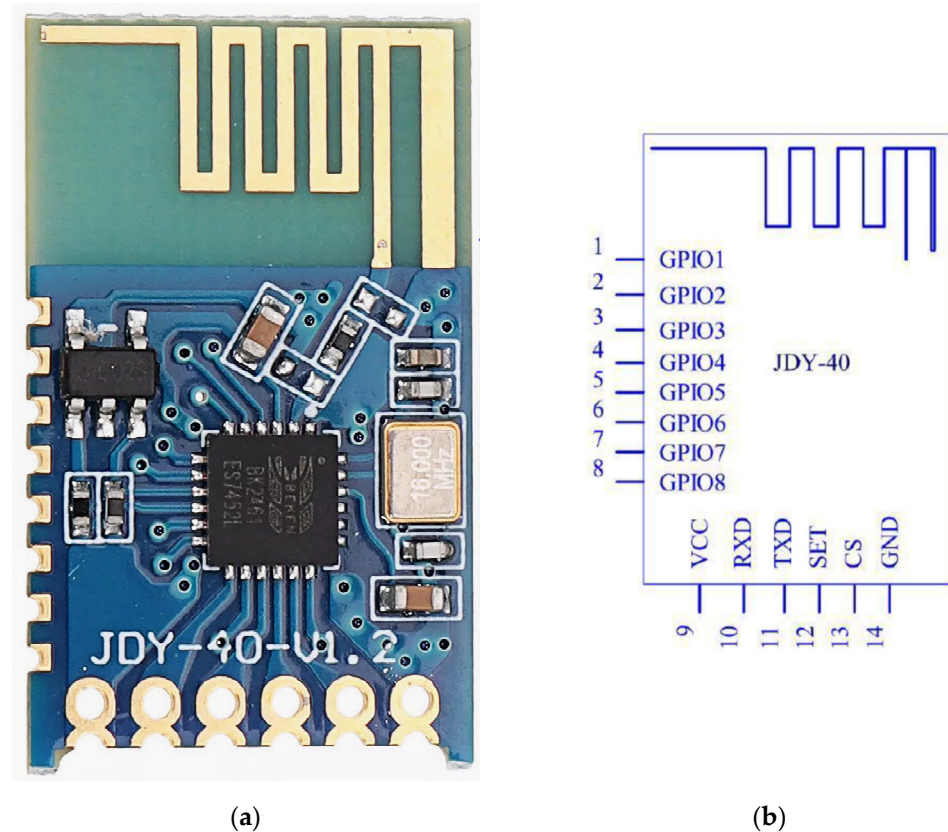


Figure 7. JDY-40 radio module: (a) appearance of JDY-40 radio module; (b) JDY-40 pin definition.

This radio module was chosen because of its ability to provide a transmission range in line-of-sight conditions of up to 120 m at low supply voltages from 2.2 to 3.6 V, its low current consumption in sleep mode—no more than 5 μ A [42], and also the convenience of connecting it to a microcontroller via the UART interface.

To power the sensors, the authors, in accordance with the concept formulated in Section 1, decided to use autonomous galvanic power supplies. The use of autonomous power supplies significantly expands the freedom of choice of installation locations for sensors in the power circuits of the SWPP, which are at different potentials in relation to the common wire, which is especially important for the series-connected batteries of the SWPP.

The choice of nickel–zinc batteries PKCELL [43] is due to their increased nominal voltage of 1.6 to 1.7 V and the absence of pulsed DC-DC converters in their composition. Such batteries are not sources of additional electromagnetic interference for the infrared radiation receiver included in the developed sensor, as well as for other control and measurement circuits of the SWPP. The nominal voltage of a battery of two such elements is ≈ 3.3 V and is ideal for powering all components of the sensor. Since most of the time, the most energy-intensive sensor module—the JDY-40 transceiver—is in sleep mode, the average current consumed by the wireless sensor does not exceed 2.4 mA, and the continuous operation time from one set of batteries is at least 1 month. When the power supply is discharged to a voltage below 3.05 V (that is, approximately two days before the failure of the most power-critical node), the sensor automatically includes the “Supply is low” signal as part of the information byte with the sensor number. This fact is continuously displayed and logged at the receiving end of the radio link along with measurement data and time stamps. Replacing the power source during a pause between transmissions of information packets takes 1 to 2 s and does not disrupt the monitoring process.

2.5. Description of the Developed Smart Wireless Sensor

The block diagram of a current and voltage sensor developed in accordance with the concept formulated in Section 2.2 is shown in Figure 8. The designations in this figure are as follows: IRR—infrared receiver, VCS—primary voltage and current sensor, ZQ1—quartz resonator, MCU—microcontroller, INT1—MCU interrupt line, PO.1–PO.3—MCU output port lines, LED—indicator LED, TX—radio transmitter, and RR—reed relay. A voltage divider made up of resistors R1 and R2, the output of which is connected to the AIN1 input of the analog comparator of the MCU, and an internal reference voltage source connected inside the MCU to the second input AIN0 of the analog comparator form a unit for monitoring the supply voltage of the MCU. The response threshold of the control unit is set using a precision construction resistor R2. The components located on the sensor board are highlighted in black, those connected externally are highlighted in blue, and those contained inside the chips are in red.

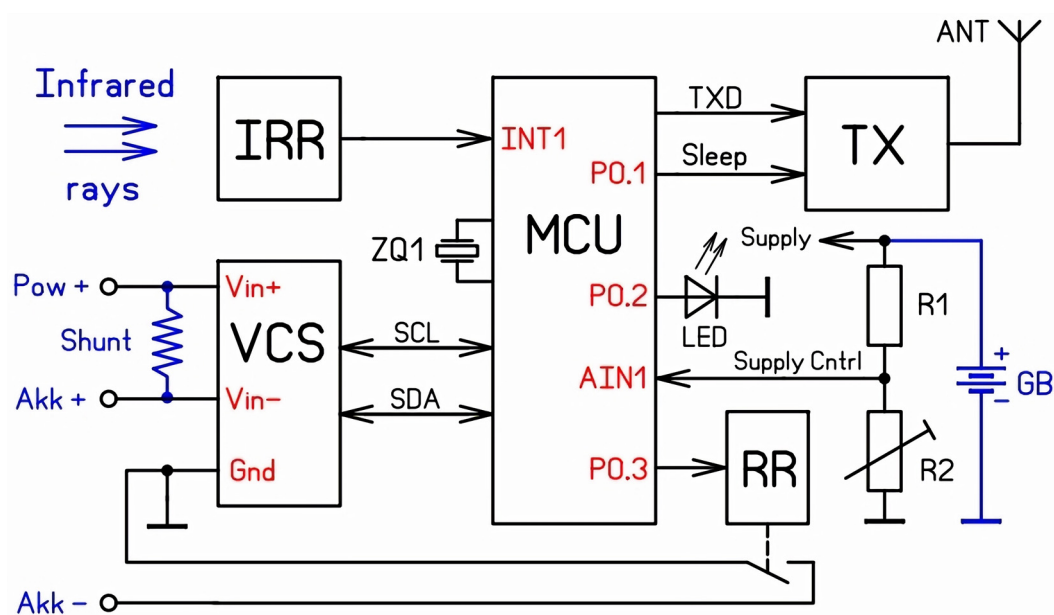


Figure 8. Block diagram of wireless current and voltage sensor.

The sensor can operate in main and diagnostic modes. In main mode, the sensor operates as follows. The TX (radio transmitter) is put into sleep mode most of the time and the RR relay contact is open. Thanks to this, the average power consumption of the sensor along the power circuit is significantly reduced, and the voltage measuring circuit practically does not consume current from the power battery. The MCU, through port INT1, cyclically polls the infrared receiver, sending reset pulses to the watchdog timer (WDT) built into the MCU at the end of the cycle. Therefore, in normal mode, the WDT does not interfere with the operation of the sensor. If the MCU freezes, for example due to strong electromagnetic interference, the WDT restarts the MCU after a set time (in our case, 512 ms), and its work according to the program automatically resumes. When a request is received from an IR request pulse generator (IR-RPG) or from an IR remote control, the microcontrollers of all sensors decipher it, but only one MCU responds to the request, having accepted the code stored in its memory. This MCU uses the RR relay contacts to connect “its” VCS to the battery for a time of about 15 to 50 ms. After the measurement process is completed, the MCU reads the current and voltage from the VCS registers. Then, the MCU of the requested sensor generates a response message containing a byte of the sensor number, two bytes of voltage, two bytes of current, and a checksum byte of the package. After which, several times in a row, it transmits a packet of several such parcels onto the airwaves at a speed of 9600 baud. During the process of measuring and transmitting the packet, the LED lights up, visualizing the sensor’s response. To transmit

a packet, the transmitter (TX) is brought out of the sleep state for 200 to 300 ms. Other wireless network sensors ignore the request that was not intended for them. Repeated transmission of information parcels and their checksum makes it possible to organize on the receiving side software detuning from reception errors in the presence of interference in the radio channel. In practice, it has been established that when using JDY-40 transceivers, to organize an uninterrupted data collection process in the SWPP ToU hardware room, it is enough to have 3–4 parcels in a package. The organization of a noise-resistant radio channel is described in more detail by the authors in [44].

If the supply voltage of the sensor drops below the set threshold, the signal at the output of the supply voltage monitoring unit changes, and the transmitter MCU adds the number 100 to the sensor number. The signal generated in this way in relation to the decrease in supply voltage is easily allocated by the MCU on the receiving side of the radio channel.

If a code is received that corresponds to a request for the sensor to enter into diagnostic mode, the MCU initiates the transmission of diagnostic data via radio. The diagnostic mode is described in more detail in Appendix B.

In the laboratory of applied electronics of Toraighyrov University (ToU), a working sample of the above-described sensor was designed and manufactured. The appearance of the sensor removed from the housing is shown in Figure 9.

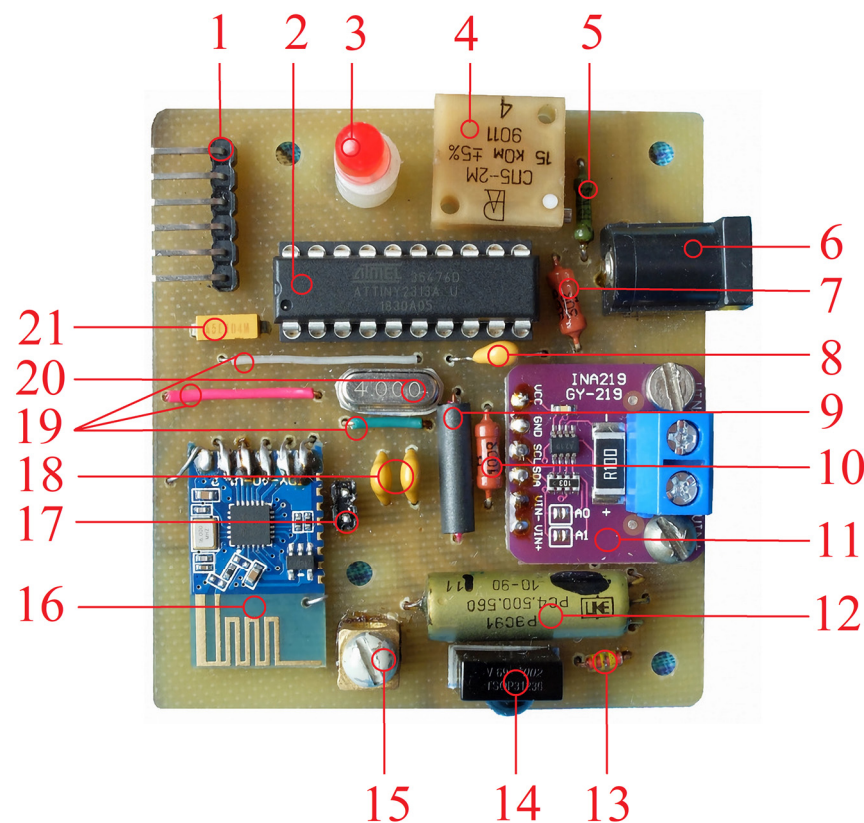


Figure 9. Appearance of wireless current and voltage sensor: connector for programmer (1), Attiny2313A microcontroller (2), LED (3), precision tuning resistor for setting power supply response threshold (4), upper arm of voltage divider that controls supply voltage (5), power supply connector (6), resistor (7), capacitor (8), throttle (9), resistor (10), INA219 current and voltage sensor (11), reed relay (12), overvoltage limiter interrupting current through relay (13), TSOP31236 infrared receiver (14), negative terminal for connecting measured voltage (15), JDY-40 radio module (16), jumper pins (17), capacitors (18), links (19), quartz resonator (20), and capacitor (21).

Tests of the above-described sensor in real conditions of the Green Energy hardware of the SWPP of ToU proved its ability to ensure error-free data transmission even through

walls over distances 4 times greater than the minimum required transmission range; so, 3 more copies of such a sensor were manufactured. Test details are given in Appendix D and Video S1: “Distance Test”.

2.6. Description of the Receiving Part of the Data Acquisition System

To organize the collection of data from several sensors in accordance with the concept formulated in Section 2.2, a full-function single-board receiver with a built-in IR request pulse generator, a real-time clock, and an informative 4-line liquid crystal display (LCD) of 20 characters was developed and manufactured in line. The block diagram of the DAS receiver is shown in Figure 10 in black.

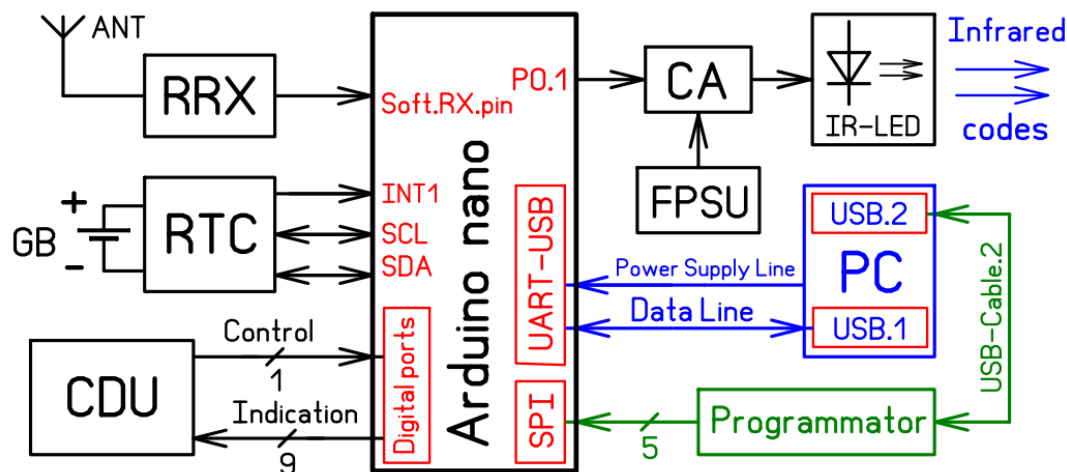


Figure 10. DAS receiver block diagram and equipment connection diagram on receiving side.

Blue shows the connection of external equipment for recording received data, while red shows the hardware resources included in the MCU platform and personal computer. The green color shows the connection of the programmer, which is necessary only during program debugging. The designations in Figure 10 are as follows: RRX—data receiver radio module, RTC—real-time clock, GB—backup battery of RTC, CDU—control and display unit, Arduino nano—microcontroller platform based on the Atmega328P MCU, Soft.RX.pin—MCU pin, on which an additional UART data input is organized in the software, INT1—MCU-level interrupt input, configured to trigger on the falling edge of the Int signal with the RTC, CA—current amplifier, FPSU—IR flash power setting unit, IR-LED—infrared LED, PC—personal computer, and USB.1 and USB.2—USB ports of a PC with virtual Com ports organized on them.

A simplified algorithm of the program that controls the operation of the DAS receiver is shown in Figure 11.

In Figure 11, in order to increase the readability of the block diagram of the algorithm, auxiliary functions and actions in interrupts are not shown. For the same purpose, the exit and entry points of the lines indicating connections between blocks are marked as “A” and “B”. The use of marks allows one to reduce the number of lines in the drawing and avoid their intersection.

The appearance of the finished DAS receiver, designed and programmed by the authors, is shown in Figure 12.

In addition to the LCD 20×4 , the control and indication unit contains two more buttons and two LEDs. The button on the board is designed to turn on/off the mode of generating IR pulses for polling sensors, and the button on the Arduino is used to restart the MCU. The red LED indicates single data reception errors, if any, and the blue is used to turn on/off the mode of generating IR pulses for polling sensors. On the LCD indicator, the symbols “!” and “” are displayed before the abbreviated designations of the sensors (D1, D2, D3, D4), and “Lo” after them. The symbol “!” before the sensor number means that

the voltage measured by it is less than the minimum permissible by the manufacturer for this battery; the symbol “~” means that the measured voltage is greater than the maximum permissible for this battery. The abbreviation “Lo” after the sensor number means that the sensor supply voltage is low (Low), less than 3.05 V. If there are no deviations in battery voltages and sensor power supply from the norm, only sensor numbers (D1, D2, D3, D4) are displayed in the top line.

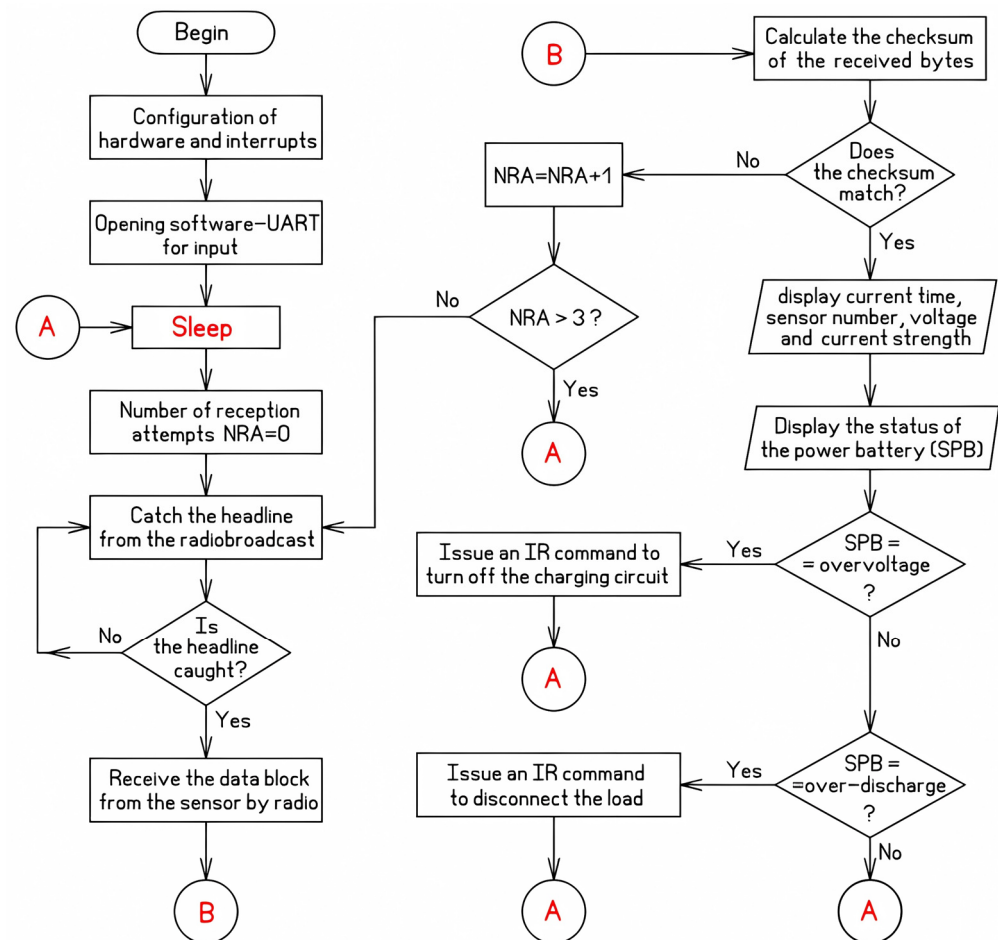


Figure 11. A simplified algorithm of the program that controls the operation of the DAS receiver.

The operation of the DAS receiver is explained by a simplified algorithm of the program that controls the operation of the DAS receiver, as shown in Figure 11. After starting the program and configuring the ports, interrupts, RTC, and I2C interface, the software UART is open for receiving radio module signals. The hardware UART-USB available on board the Arduino platform is used for two-way communication with a personal computer. In this case, its input line is used to set the current RTC date and time, and its output line is used to log the operation of the DAS on the computer. After this, the receiver goes into sleep mode. When an interrupt signal is received, generated every second by the RTC chip, the receiver MCU generates an IR code to request a response from the sensor, after which the receiver switches from sleep mode to the mode of detecting the header of the data block sent by the sensor. After receiving the header, the MCU receives data from the sensor, decrypts them, adds time and date stamps to them, displays them on the LCD indicator, and sends them to the PC for display on the monitor and recording on the hard drive. The process is then repeated cyclically for the remaining sensors.

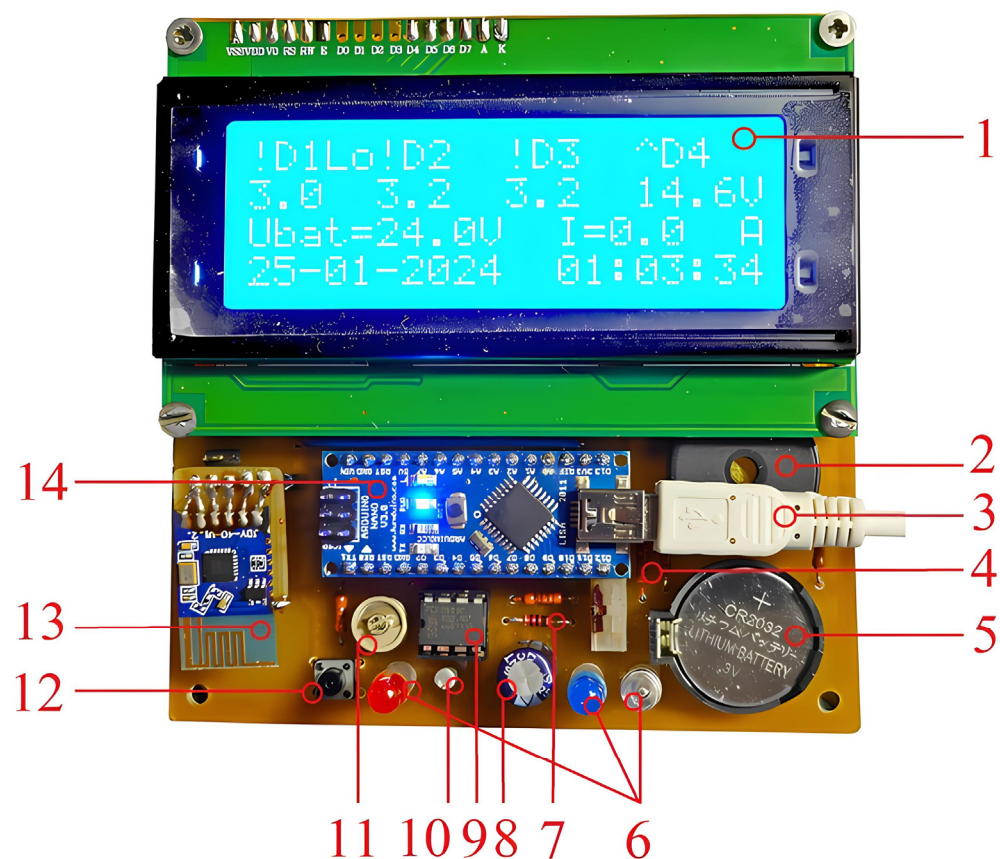


Figure 12. Appearance of DAS receiver removed from case: LCD (1), buzzer (2), USB cable (3), resistor (4), backup battery for powering RTC (5), LED (6), diode (7), oxide semiconductor capacitor (8), RTC chip (9), quartz resonator RTC (10), tuning capacitor (11), button to turn on/off mode of generating IR pulses for polling sensors (12), receiver radio module (13), and microcontroller platform Arduino nano (14).

If an overcharge or overdischarge of at least one of the SWPP batteries is detected, the receiver MCU generates and sends IR codes to the DC of the IRC command decoder, as shown in Figure 2. Commands from the decoder are sent to the corresponding EU of backup protection located on the side where the batteries are located, thus preventing failure or a reduction in battery life. A time delay in cases where it is necessary before executing a particular command is set in the EU. The mentioned DC and EU perform based on the known principles of IR remote control and are therefore not described in this article.

The control program allows you to poll several dozen sensors with an interval of 1 s, which is enough to organize full monitoring of the operation of the SWPP of ToU. At the same time, the absence of a response from any number of sensors does not lead to failures in receiving data from other sensors. The return of sensors to the system is detected and displayed automatically. If necessary, the polling frequency can be increased to 2 times per second by simply reconfiguring the interrupt period from the RTC.

3. Results and Discussion

Figures 13 and 14 show screenshots of the process of monitoring the voltage and current of four series-connected SWPP batteries. When recording them, the voltage deviation of individual batteries was simulated by temporarily replacing the corresponding battery with a regulated laboratory power source.

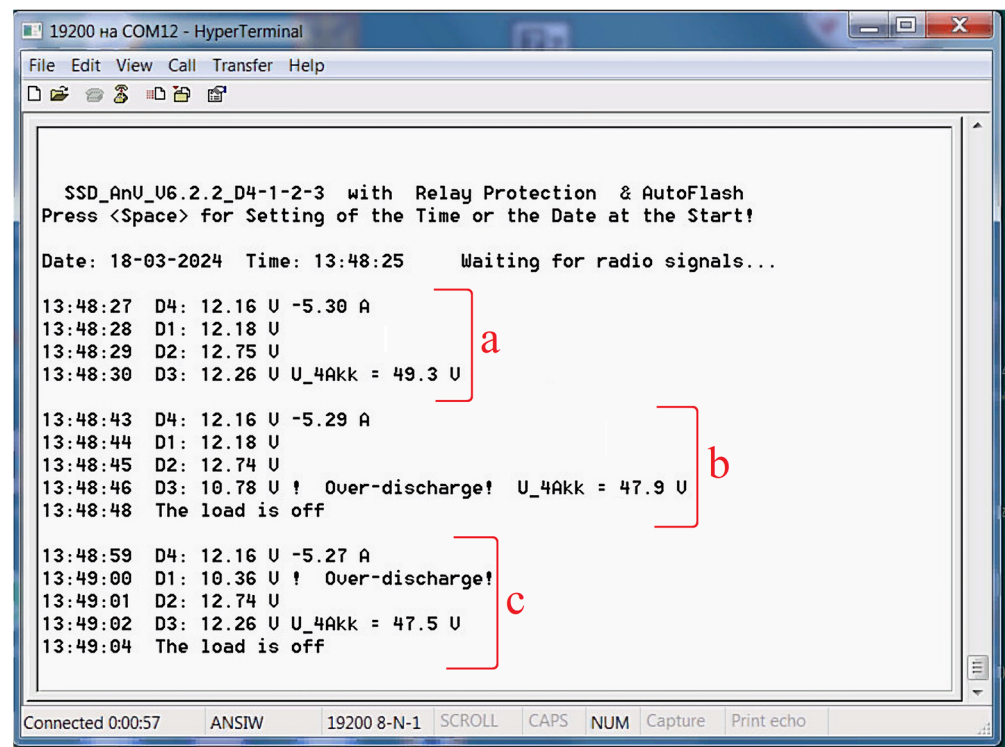


Figure 13. A screenshot of the process of monitoring the voltage and current of SWPP batteries.



Figure 14. A screenshot of the process of monitoring the voltage and current of SWPP batteries with a recorded case of overcharging battery No. 2.

Figure 13a shows the nature of the recorded information at permissible voltages (12–14 V) of the power batteries. Backup protection is not required in this case. Figure 13b,c show the system's reaction to overdischarge of the first and third batteries below the permissible limit (<12 V). In both of these cases, to prevent battery failure, backup protection issued a command via an infrared channel to turn off the load (or switch it to power from the city network). It should be emphasized that backup protection is triggered only in cases where the standard controllers of solar panels and wind generators for some reason cannot ensure normal operation of the batteries.

If the battery was overcharged above the permissible limit (>14 V), the system issued an IR command to turn off the charging circuit of the entire section of series-connected power batteries, as shown in Figure 14. If it is necessary to organize backup protection and against short circuits, faster equipment should be used.

As a result of the research, the authors formulated the principles of constructing a wireless DAS for low-power GEPPs free from some of the disadvantages of analogues, and developed and implemented “in hardware” a wireless intelligent current and voltage sensor and equipment for indicating and recording data received from several such sensors. Successful tests of the DAS organized in this way in the hardware room of the “Green Energy” power plant of ToU confirmed the correctness of the design principles, circuit solutions, and program algorithms embedded in the developed system. The distance from the installation sites of the sensors to the installation site of the receiving equipment in the equipment room does not exceed 4.5 m; so, the result of the range tests should be

interpreted as the possibility of error-free data reception using the described equipment with a four-fold margin in range. Appendix D and Video S1: “Distance Test” illustrates the range of the sensor.

In addition to solving the main problem of organizing wireless data collection, the authors managed to provide many additional useful functions that were not available in known analogues:

- The use of an infrared communication channel in the described DAS in addition to the radio channel makes it possible not only to organize a feedback channel with SWPP equipment protected from outside interference, but also to implement on this basis backup protection of SWPP equipment from damage and abnormal operating conditions (PDAOCs). In the future, this will make it possible to transform the data collection system into a full-fledged automatic control system (ACS) for the operation of the SWPP with relay protection functions for all of the main elements of the SWPP.
- The construction of sensors and other equipment based on mass-produced, widely available electronic components and modules facilitates the organization of their mass production.
- Powering the sensors from autonomous sources that are not galvanically connected to power circuits, as well as the wireless method of transmitting information, makes it possible to avoid a “web” of wires near the power circuits of the SWPP and thus minimizes their influence on the measuring circuits and recording equipment.
- The use of autonomous power supplies for sensors significantly expands the freedom of choice of their installation locations in the power circuits of the SWPP, which are at different potentials in relation to the common wire, which is especially important, for example, for series-connected SWPP batteries.
- Connecting the voltage measuring circuits of the sensors to the batteries only for the duration of the measurement automatically eliminates the problem of preventing damage to the SWPP batteries due to their deep discharge during a long-term shortage of solar and wind energy or during temporary conservation of the SWPP. This is particularly relevant for GEPPs with low-capacity batteries. The resource of reed relays allows us in our case to carry out such switching for several decades [45].
- The hardware anti-freeze protection built into the sensors and the DAS receiver prevents disruptions to the monitoring processes and operation of the ACS and PDAOC due to interference that occurs during switching in the power circuits of the SWPP or in the supply network.
- The developed sensors contain tools for rapid diagnoses of their serviceability and control of the main parameters of their settings. The diagnostic process can be initiated at almost any time using the hand-held IR remote control. This does not require disconnecting the sensors from the SWPP circuits and connecting additional wires to them.

An analysis of the current level of technology developed for remote intervention in the operation of control systems led the authors to the conclusion that reliable protection against harmful influences should be ensured by developing equipment whose operation is hardware-independent of the Internet. In the system proposed by the authors, the process of remote data collection is protected from outside interference not only in software, but also in hardware due to the refusal to exchange critical information, from the point of view of hacking, over radio channels. The transmission of requests to sensors and control actions on the power equipment is carried out exclusively via the IR channel. With this approach, even deliberately clogging the radio channel with powerful interference will only pause the monitoring process, but will not lead to the issuance of false control actions on the power equipment of the GEPP.

For clarity, the significant differences of the proposed system are summarized in Table 1.

Table 1. Comparison of some features of existing and proposed data acquisition systems.

Types of GEPP Monitoring Systems \ Monitoring Functions	Possibility of Measuring the Voltage of Each of the Series-Connected Batteries	Automatic Response to Malfunctions and Abnormal Operating Modes of GEPPs	Independence of DAS from the Quality of the Internet and Cyber-Attacks	Automatic Connection of Additional Load in Case of Excess Natural Energy	Availability of Online Remote Diagnostics of the State of SSD Components	Absence of a “Web of Wires” near GEPP Power Circuits
Monitoring of GEPP using GSM	–	–	+ / –	–	–	–
Monitoring of GEPP based on Zigbee	+	–	+ / –	–	–	+
Monitoring of GEPP based on Internet of Things	+ / –	–	–	–	–	–
Monitoring of GEPP using Bluetooth	–	–	+	–	–	–
Monitoring of GEPP using Wi-Fi	–	–	–	–	–	–
Monitoring of GEPP using radio and IR channels	+	+	+	+	+	+

4. Conclusions

In this article, the authors propose the concept of building a wireless DAS, free from some of the disadvantages of analogues and which has additional useful functions in comparison with them. The structure of the main DAS module, the design of intelligent wireless sensors, and a method for connecting them to the main module have been developed, significantly reducing the number and length of connecting wires.

The use of an infrared communication channel in the described DAS in addition to the radio channel made it possible to organize a feedback channel protected from outside interference with the sensors and power equipment of the SWPP. On this basis, the following was achieved:

- (1) Implement backup protection of SWPP batteries from overcharge and overdischarge;
- (2) Introduce into the system elements to increase the efficiency of natural energy use by automatically switching part of the SWPP loads from power from the public power grid to power from natural energy when there is an excess of it and vice versa when there is a lack of it;
- (3) Organize prompt remote diagnostics of the status of sensors without connecting additional wires.

In the future, this will make it possible to transform the data collection system into a full-fledged automatic control system for the operation of the SWPP with the functions of backup protection of the main elements of the SWPP against damage and abnormal operating conditions, adapted for effective collaboration with existing utility power supply networks.

Successful full-scale tests of the developed system in the “Green Energy” hardware room of the Toraighyrov University SWPP proved its full functionality and the correctness of the design principles and technical solutions underlying it. The concept of constructing the DAS proposed in this article is suitable for constructing systems for the remote measurement and logging of almost any physical quantity and makes it possible to easily

increase the number of interrogated sensors to several dozen; so, the scope of application of the described DAS can be significantly expanded.

Supplementary Materials: The following supporting information can be downloaded at: <https://www.mdpi.com/article/10.3390/app14135553/s1>, Video S1: Distance Test.

Author Contributions: Conceptualization, A.M. (Anatoliy Manukovsky); data curation, A.M. (Anatoliy Manukovsky); formal analysis, A.K.; funding acquisition, A.S.; investigation, A.M. (Anatoliy Manukovsky) and A.S.; methodology, A.K. and O.T.; project administration, A.S.; resources, A.M. (Alexey Manukovsky); software, A.M. (Anatoliy Manukovsky); supervision, A.K. and O.T.; validation, A.M. (Anatoliy Manukovsky), A.S. and A.M. (Alexey Manukovsky); visualization, A.M. (Alexey Manukovsky); writing—original draft, A.S.; writing—review and editing, O.T. All authors have read and agreed to the published version of the manuscript.

Funding: This study was funded by the Committee of Science of the Ministry of Science and Higher Education of the Republic of Kazakhstan (grant no. AP15473220).

Institutional Review Board Statement: Not applicable.

Informed Consent Statement: Not applicable.

Data Availability Statement: The original contributions presented in the study are included in the article, further inquiries can be directed to the corresponding author.

Conflicts of Interest: The authors declare no conflicts of interest.

Appendix A

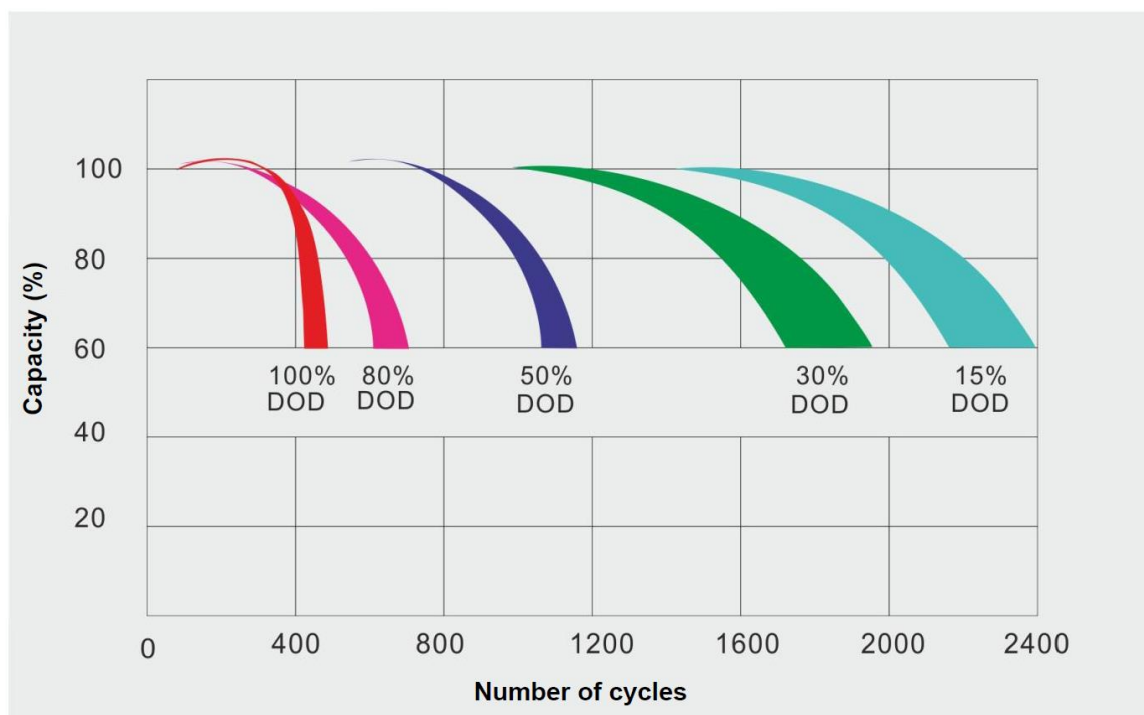


Figure A1. The dependence of the number of cycles on the discharge depth.

Appendix B

The diagnostic mode is intended for online remote diagnosis of the health of sensors and for the monitoring of the main parameters of their settings without disconnecting the sensors from the SWPP circuits and without connecting additional wires to them. It is initiated separately for each sensor using a standard infrared remote control in pauses between sensor polling pulses from the IR-RPG, or when the latter is temporarily turned off. Diagnostic results are received remotely using a standard radio module and displayed

on a laptop screen using a standard TTL-USB adapter or on a smartphone screen using a Bluetooth module. Examples of sensor responses to diagnostic data requests are shown in Figure A2.

Terminal log file

```
-----
Sender_2.4 V.4.9 - TOK by Sensor #2 is NOT Measured !
Press 2-nd button in the penultimate Row of the IR-Pult for output U2!
Config_2: 2EEE  Calibr= 0000, 10U= -6 mV  Low Supply Voltage!

Sender_2.4 V.4.9 - TOK by Sensor #3 is NOT Measured !
Press 3-rd button in the penultimate Row of the IR-Pult for output U3!
Config_3: 2EEE  Calibr= 0000, 10U= 0 mV

Sender_2.4 V.4.9 for Sensor #4 & Shunt= 15A
Press 4-th button in the penultimate Row of the IR-Pult for output U4 & I4!
Config_4: 2EEF,  Calibr= 8664  10U= -1 mV
-----
End log file
```

Figure A2. Examples of sensor responses to diagnostic data requests.

In the first of the examples given, the supply voltage of sensor No. 2 is less than 3.05 V, which is reflected in the fifth line of the log file of the message “Low supply voltage!”, underlined in red. Sensors No. 2 and No. 3 are configured to measure voltage only, and No. 4 is configured to measure voltage and current up to 15 A with an external shunt.

Appendix C

1. At the beginning of the program, the values of the INA219 sensor configuration registers are selected for the following reasons:

In the bottom line of Table A1, there are values of the configuration register bits that we selected (highlighted in red) in accordance with the recommendations from the following fragments of the INA219 datasheet.

All INA219 16-bit registers are actually two 8-bit bytes via the I2C interface.

Table A1. Configuration register 00h (read/write).

BIT #	D15	D14	D13	D12	D11	D10	D9	D8	D7	D6	D5	D4	D3	D2	D1	D0
BIT NAME	RST	—	BRNG	PG1	PG0	BADC4	BADC3	BADC2	BADC1	SADC4	SADC3	SADC2	SADC1	MODE3	MODE2	MODE1
POR VALUE	0	0	1	0	1	1	1	0	1	1	1	0	1	1	1	1

Table A2. Bit descriptions.

RST:	Reset Bit
Bit 15	Setting this bit to ‘1’ generates a system reset that is the same as power-on reset. This resets all registers to default values; this bit self-clears.
BRNG:	Bus Voltage Range
Bit13	0 = 16 V FSR 1 = 32 V FSR (default value)

Table A2. *Cont.*

PG:	PGA (Shunt Voltage Only)
Bits 11, 12	This sets PGA gain and range. Note that the PGA defaults to $\div 8$ (320 mV range). Table A3 shows the gain and range for the various product gain settings.
BADC:	BADC BusADC Resolution/Averaging
Bits 7–10	These bits adjust the Bus ADC resolution (9-, 10-, 11-, or 12-bit) or set the number of samples used when averaging the results for the Bus Voltage Register (02h).
SADC:	SADC Shunt ADC Resolution/Averaging
Bits 3–6	These bits adjust the shunt ADC resolution (9-, 10-, 11-, or 12-bit) or set the number of samples used when averaging the results for the Shunt Voltage Register (01h). BADC (Bus) and SADC (Shunt) ADC resolution/averaging and conversion time settings are shown in Table A4.
MODE:	Operating Mode
Bits 0–2	This selects continuous, triggered, or power-down mode of operation. These bits default to continuous shunt and bus measurement mode. The mode settings are shown in Table A5.

Table A3. PG Bit Settings ⁽¹⁾.

PG1	PG0	GAIN	RANGE
0	0	1	± 40 MV
0	1	+2	± 80 MV
1	0	+4	± 160 MV
1	1	+8	± 320 MV

⁽¹⁾ Shaded values are default.**Table A4.** ADC settings ⁽¹⁾.

ADC4	ADC3	ADC2	ADC1	Mode/Samples	Conversion Time
0	X ⁽²⁾	0	0	9-bit	84 μ s
0	X ⁽²⁾	0	1	10-bit	148 μ s
0	X ⁽²⁾	1	0	11-bit	276 μ s
0	X ⁽²⁾	1	1	12-bit	532 μ s
1	0	0	0	12-bit	532 μ s
1	0	0	1	2	1.06 ms
1	0	1	0	4	2.13 ms
1	0	1	1	8	4.26 ms
1	1	0	0	16	8.51 ms
1	1	0	1	32	17.02 ms
1	1	1	0	64	34.05 ms
1	1	1	1	128	68.10 ms

⁽¹⁾ Shaded values are default. ⁽²⁾ X = Do not care.

Table A5. Mode settings ⁽¹⁾.

Mode 3	Mode 2	Mode 1	Mode
0	0	0	Power-Down
0	0	1	Shunt Voltage, Triggered
0	1	0	Bus Voltage, Triggered
0	1	1	Shunt and Bus, Triggered
1	0	0	ADC Off (disabled)
1	0	1	Shunt Voltage, Continuous
1	1	0	Bus Voltage, Continuous
1	1	1	Shunt and Bus, Continuous

⁽¹⁾ Shaded values are default.

Bits 15 and 14 are left at their default values of 0.

Bit 13 for the 32 V bus = 1.

Bits 12 and 11 are used for the voltage drop across 80 mV shunt = 01.

Bits 10 to 7 and 6 to 3 according to Table A4 for 32 samples with a 12-bit resolution are chosen equal to 1101.

For sensors that measure the current as well as the voltage, according to Table A5, for operating mode = shunt and bus and continuous bits 2 to 0, select conditions 111. The result of selecting the bits of the configuration register will be entered in the bottom row of Table A1.

Contents of the Config register = 0010.1110.1110.1111 = 2EEF (Hex).

For sensors that measure only the voltage, according to Table A5, for operating mode = bus voltage, continuous bits 2 to 0 are selected equal to 110.

Contents of the configuration register for these sensors = 0010.1110.1110.1110 = 2EEE (Hex).

2. To calculate the Calibr INA219 register, the program shown in Figure 4 performs the following steps:

In the case of using an external shunt, the program calculates the resistance of the external shunt using the rated current and voltage drop across the shunt using Ohm's law, and then calculates the total resistance of the parallel-connected internal and external shunts using the well-known equation, Formula (A1):

$$R_{shunt} = \frac{R_{internal\ shunt} \cdot R_{external\ shunt}}{R_{internal\ shunt} + R_{external\ shunt}}. \quad (A1)$$

In our case, it turns out that $R_{shunt} \approx 4762 \cdot 10^{-3}$ Ohm. The program then calculates the value of Current_LSB—(least significant bit—the value of the least significant bit of the register) for the Calibr register using Formula (A2):

$$I_{LSB} = \frac{I_{maximum\ expected}}{2^{15}} = \frac{15\ A}{32768} = 0.000458\ A. \quad (A2)$$

We select and enter into the program the nearest round value of $I_{LSB} = 1$ mA. The program calculates the maximum displayed current value, which fits into a 16-bit number, $I_{max} = 32.768$ A. To obtain a value of 15 A in the current register at Config = 399F Hex (320 mV on the shunt), the register value is calculated using the formula from the datasheet (A3):

$$Calibr = \text{trunk} \left(\frac{0.04096}{I_{LSB} \times R_{SHUNT}} \right) = 8601 \quad (A3)$$

To obtain a value of 15 A in the current register at Config = 2EEF Hex (80 mV on the shunt), the Cal value is recalculated:

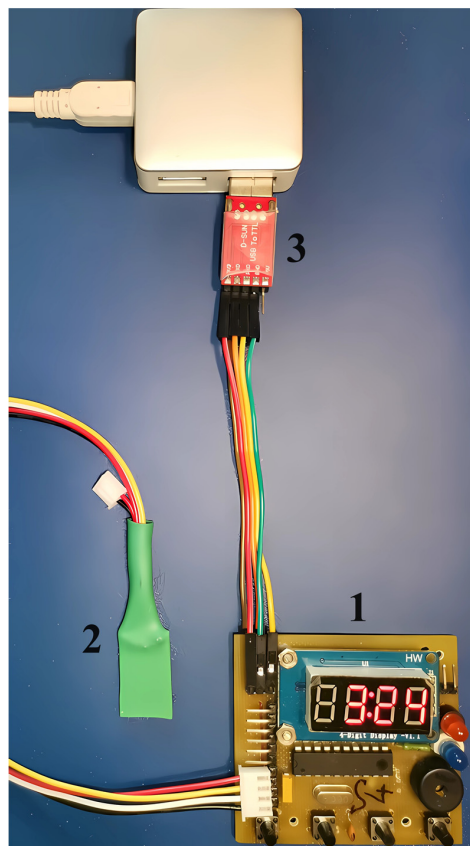
$$Calibr = \frac{8601 \cdot 320}{80} = 34404 = 8664\ Hex \quad (A4)$$

After calibrating the current channel using a standard ammeter, the value 31,300 = 7A44 Hex is accepted for firmware in the “Calibr” register.

Appendix D

To test the performance of the above-described sensor and determine its range in real conditions of the SWPP ToU hardware, a simplified receiver of its signals was designed and built, not containing a real-time clock (RTC) and IR-RPG. This work was based on the technical solutions and algorithm formulated in [44]. The appearance of the testing equipment on the receiving side is shown in Figure A3a. In Figure A3a, number 1 indicates the sensor signal receiver on the Attiny2313A MCU, number 2 indicates the radio module of the JDY-40 transceiver, and number 3 indicates the TTL-USB converter connected via USB-HUB to a personal computer (PC).

To determine the maximum range of data transmission, a program was installed in the sensor microcontroller that implements the mode of continuous automatic measurement and the cyclic transmission of measured values to the receiving and recording device. The sensor with an SWPP battery simulator and an SWPP load simulator in the form of a miniature incandescent lamp connected to it gradually moved away from the receiving set of equipment. Using the “Terminal V.9b” program on a PC, time stamps were generated and the voltage and current of the battery and load simulators received over the radio channel, measured by the sensor, were generated and recorded in a file. Fragments of received data recorded as the distance increases are shown in Figure A3b, with the upper lines corresponding to a sensor distance of 5 m, and the bottom lines representing a distance of 20 m. The minus sign in front of the current value indicates the battery discharge mode.



(a)

```

Range test from 5 to 18meter log
Terminal log file
Date: 02.10.2023 - 13:02:51
-----
13:02:57.859> 4: 5073 mV, -78 mA.
13:03:08.265> 4: 5073 mV, -78 mA.
13:03:18.671> 4: 5073 mV, -78 mA.
13:03:29.078> 4: 5073 mV, -78 mA.
13:03:39.484> 4: 5073 mV, -78 mA.
13:03:49.890> 4: 5073 mV, -78 mA.
13:04:00.234> 4: 5069 mV, -78 mA.
13:04:10.640> 4: 5073 mV, -78 mA.
13:04:21.046> 4: 5069 mV, -78 mA.
13:04:31.421> 4: 5073 mV, -78 mA.
13:04:41.859> 4: 5069 mV, -78 mA.
13:04:52.234> 4: 5069 mV, -78 mA.
13:05:02.609> 4: 5069 mV, -78 mA.
.
.
.
13:33:58.515> 4: 5025 mV, -78 mA.
13:34:08.921> 4: 5025 mV, -78 mA.
13:34:19.328> 4: 5025 mV, -78 mA.
13:34:29.734> 4: 5025 mV, -78 mA.
13:34:40.140> 4: 5021 mV, -78 mA.
13:34:50.484> 4: 5021 mV, -78 mA.
13:35:00.890> 4: 5029 mV, -78 mA.
13:35:11.296> 4: 5021 mV, -78 mA.
13:35:21.703> 4: 5021 mV, -78 mA.
13:35:32.109> 4: 5029 mV, -78 mA.
13:35:42.453> 4: 5025 mV, -78 mA.
13:35:52.859> 4: 5029 mV, -78 mA.
13:36:03.265> 4: 5025 mV, -78 mA.
13:36:13.671> 4: 5025 mV, -78 mA.
13:36:24.078> 4: 5025 mV, -78 mA.
13:36:34.484> 4: 5033 mV, -78 mA.
13:36:44.828> 4: 5025 mV, -78 mA.
13:36:55.234> 4: 5029 mV, -78 mA.
13:37:05.640> 4: 5021 mV, -78 mA.
13:37:16.046> 4: 5029 mV, -78 mA.
13:37:26.453> 4: 5033 mV, -78 mA.
13:37:36.859> 4: 5029 mV, -78 mA. #
13:37:57.640> 4: 5029 mV, -78 mA.
13:38:08.046> 4: 5025 mV, -78 mA.
-----
Date: 02.10.2023 - 13:51:38
End log file

```

(b)

Figure A3. The appearance of the testing equipment on the receiving side and the results of testing the system for the transmission range: the appearance of the testing equipment on the receiving side (a); fragments of the received data recorded as the distance increases (b).

The testing equipment made it possible to record in a log file a protocol for receiving signals from a wireless sensor as it gradually moved away from the set of receiving equipment at a distance from 5 to 20 m. The receding rate was kept constant throughout the experiment, so that given the starting and final distances, the transmission distance could be determined for any time recorded in the log file. If even one erroneous parcel is received out of four sent in a row, the receiver software automatically issues a “#” sign to the terminal. The absence of such a sign in the line means full compliance of the received data with the transmitted data.

Analysis of the log file shows that single reception errors (automatically marked with a “#”) began at 13:37:37, when the sensor was moved outside the Green Energy equipment room to the far end of the corridor, and the signal was transmitted through two internal reinforced concrete walls.

The distance from the sensor installation sites to the receiving equipment installation site in the equipment room did not exceed 4.5 m; therefore, the result of the range tests should be interpreted as the possibility of error-free data reception using the described equipment with a four-fold range margin.

References

- Jaen-Cuellar, A.Y.; Elvira-Ortiz, D.A.; Osornio-Rios, R.A.; Antonino-Daviu, J.A. Advances in Fault Condition Monitoring for Solar Photovoltaic and Wind Turbine Energy Generation: A Review. *Energies* **2022**, *15*, 5404. [\[CrossRef\]](#)
- Roy, P.; He, J.; Zhao, T.; Singh, Y.V. Recent Advances of Wind-Solar Hybrid Renewable Energy Systems for Power Generation: A Review. *IEEE Open J. Ind. Electron. Soc.* **2022**, *3*, 81–104. [\[CrossRef\]](#)
- Antonio Barrozo Budes, F.; Valencia Ochoa, G.; Obregon, L.G.; Arango-Manrique, A.; Ricardo Núñez Álvarez, J. Energy, Economic, and Environmental Evaluation of a Proposed Solar-Wind Power On-Grid System Using HOMER Pro®: A Case Study in Colombia. *Energies* **2020**, *13*, 1662. [\[CrossRef\]](#)
- Sovacool, B.K. The Intermittency of Wind, Solar, and Renewable Electricity Generators: Technical Barrier or Rhetorical Excuse? *Util Policy* **2009**, *17*, 288–296. [\[CrossRef\]](#)
- Madeti, S.R.; Singh, S.N. A Comprehensive Study on Different Types of Faults and Detection Techniques for Solar Photovoltaic System. *Sol. Energy* **2017**, *158*, 161–185. [\[CrossRef\]](#)
- Bharath Kurukuru, V.S.; Blaabjerg, F.; Khan, M.A.; Haque, A. A Novel Fault Classification Approach for Photovoltaic Systems. *Energies* **2020**, *13*, 308. [\[CrossRef\]](#)
- Manukovskii, A.V.; Sagyndyk, A.B. Selection of Current Sensors for Monitoring of Working of Solar-Wind Power Plants. *Bull. Toraighyrov Univ. Energetics Ser.* **2022**, 212–225. [\[CrossRef\]](#)
- Manukovskii, A.V.; Zhakupov, N.R.; Begancova, M.; Zhumabaj, N. Increasing the Efficiency of Using Renewable Energy Mini-Power Plants. *Molod. Uchenyj* **2018**, *33*, 19–22.
- Henze, N.; Bendel, C.; Fruchting, A.; Kirchhof, J. Application of photovoltaic solar cells in planar antenna structures. In Proceedings of the 3rd World Conference on Photovoltaic Energy Conversion, Osaka, Japan, 11–18 May 2003; Volume 1, pp. 220–223.
- Wang, W.; Xu, Y.; Khanna, M. A Survey on the Communication Architectures in Smart Grid. *Comput. Netw.* **2011**, *55*, 3604–3629. [\[CrossRef\]](#)
- Eke, R.; Sertap Kavasoglu, A.; Kavasoglu, N. Design and Implementation of a Low-Cost Multi-Channel Temperature Measurement System for Photovoltaic Modules. *Measurement* **2012**, *45*, 1499–1509. [\[CrossRef\]](#)
- Carullo, A.; Vallan, A. Outdoor Experimental Laboratory for Long-Term Estimation of Photovoltaic-Plant Performance. *IEEE Trans. Instrum. Meas.* **2012**, *61*, 1307–1314. [\[CrossRef\]](#)
- Zidani, C.; Benyoucef, B.; Madini, N. Exergetic Assessment of Transmission-Concentrated Solar Energy Systems via Optical Fibres for Building Applications. *Int. J. Exergy* **2012**, *11*, 216. [\[CrossRef\]](#)
- Kribus, A.; Zik, O.; Karni, J. Optical Fibers and Solar Power Generation. *Sol. Energy* **2000**, *68*, 405–416. [\[CrossRef\]](#)
- Kandilli, C.; Ulgen, K. Review and Modelling the Systems of Transmission Concentrated Solar Energy via Optical Fibres. *Renew. Sustain. Energy Rev.* **2009**, *13*, 67–84. [\[CrossRef\]](#)
- Han, J.; Choi, C.; Park, W.; Lee, I.; Kim, S. PLC-Based Photovoltaic System Management for Smart Home Energy Management System. *IEEE Trans. Consum. Electron.* **2014**, *60*, 184–189. [\[CrossRef\]](#)
- Han, J.; Jeong, J.-D.; Lee, I.; Kim, S.-H. Low-Cost Monitoring of Photovoltaic Systems at Panel Level in Residential Homes Based on Power Line Communication. *IEEE Trans. Consum. Electron.* **2017**, *63*, 435–441. [\[CrossRef\]](#)
- Tejwani, R.; Kumar, G.; Solanki, C. Remote Monitoring for Solar Photovoltaic Systems in Rural Application Using GSM Voice Channel. In Proceedings of the Energy Procedia; Elsevier Ltd.: Amsterdam, The Netherlands, 2014; Volume 57, pp. 1526–1535.
- Mahjoubi, A.; Fethi Mechlouch, R.; Ben Brahim, A. A Low Cost Wireless Data Acquisition System for a Remote Photovoltaic (PV) Water Pumping System. *Energies* **2011**, *4*, 68–89. [\[CrossRef\]](#)

20. Nkoloma, M.; Zennaro, M.; Bagula, A. SM²: Solar monitoring system in Malawi. In Proceedings of the ITU Kaleidoscope 2011: The Fully Networked Human?—Innovations for Future Networks and Services (K-2011), Cape Town, South Africa, 12–14 December 2011; pp. 1–6.
21. Shariff, F.; Rahim, N.A.; Hew, W.P. Zigbee-Based Data Acquisition System for Online Monitoring of Grid-Connected Photovoltaic System. *Expert Syst. Appl.* **2015**, *42*, 1730–1742. [\[CrossRef\]](#)
22. Batista, N.C.; Melício, R.; Matias, J.C.O.; Catalão, J.P.S. Photovoltaic and Wind Energy Systems Monitoring and Building/Home Energy Management Using ZigBee Devices within a Smart Grid. *Energy* **2013**, *49*, 306–315. [\[CrossRef\]](#)
23. Anwari, M.; Hidayat, A.; Hamid, M.I. Taufik Wireless Data Acquisition for Photovoltaic Power System. In Proceedings of the INTELEC 2009—31st International Telecommunications Energy Conference, Incheon, Republic of Korea, 18–22 October 2009; IEEE: Piscataway, NJ, USA, 2009; pp. 1–4.
24. Prasanna Rani, D.D.; Suresh, D.; Rao Kapula, P.; Mohammad Akram, C.H.; Hemalatha, N.; Kumar Soni, P. IoT Based Smart Solar Energy Monitoring Systems. *Mater. Today Proc.* **2023**, *80*, 3540–3545. [\[CrossRef\]](#)
25. Pulungan, A.B.; Risfendra, R.; Purwanto, W.; Maksum, H.; Setiawan, O. Design and development of real time monitoring single axis solar tracker by using internet of things. *Int. J. GEOMATE* **2020**, *18*, 81–87. [\[CrossRef\]](#)
26. Hasib Cheragee, S.; Hassan, N.; Ahammed, S.; Touhidul Islam, A.Z. A Study of IoT Based Real-Time Solar Power Remote Monitoring System. *Int. J. Ambient Syst. Appl.* **2021**, *9*, 27–36. [\[CrossRef\]](#)
27. Barka, C.; Messaoudi-Abid, H.; Setthom, H.B.A.; Bennani-Ben Abdelghani, A.; Slama-Belkhodja, I.; Sammoud, H. A Real Time, Wireless and Low Cost Data Acquisition System for Residential PV Modules. In Proceedings of the 6th IEEE International Energy Conference (ENERGYCon), Gammarth, Tunisia, 28 September–1 October 2020; Institute of Electrical and Electronics Engineers Inc.: Piscataway, NJ, USA, 2020; pp. 417–422.
28. Wang, Y.; Wen, H.; Hou, X.; Tang, H.; Sun, H.; Zheng, K.; Li, S. Comparison of Differential-Mode and Mixed-Mode Conducted Emission for Household Appliances in Power-Line Communication System. *IEEE Trans. Electromagn. Compat.* **2017**, *59*, 2023–2028. [\[CrossRef\]](#)
29. Card, J. TS 151 013—V18.0.0—Digital Cellular Telecommunications System (Phase 2+) (GSM); Test Specification for Subscriber Identity Module (SIM) Application Programming Interface (API) for Java Card (3GPP TS 51.013 Version 18.0.0 Release 18); 2024. Available online: <https://cdn.standards.iteh.ai/samples/71720/5e17ba0d49d241a4aafc9a5a36e1875/ETSI-TS-151-013-V18-0-0-2024-05-.pdf> (accessed on 29 May 2024).
30. ZigBee Modules Cut Development of ZigBee Compatible Products in Half. Available online: <https://wireless-e.ru/radiomoduli/moduli-zigbee/> (accessed on 25 May 2024).
31. HC-12 Datasheet(PDF) 5 Page—List of Unclassified Manufacturers. Available online: <https://html.alldatasheet.com/html-pdf/1242982/ETC1/HC-12/573/5/HC-12.html> (accessed on 25 May 2024).
32. How Tonight’s Geomagnetic Storm Could Send GPSs Haywire and Cause Havoc for Airplanes—Here’s What Could Happen to Cell Phones or Other Electronics. Available online: <https://www.dailymail.co.uk/sciencetech/article-13404635/what-happen-geomagnetic-storm-hits-TODAY-US.html> (accessed on 21 May 2024).
33. Russia: Telegram Block Leads to Widespread Assault on Freedom of Expression Online. Available online: <https://www.penninternational.org/news/russia-telegram-block-leads-to-widespread-assault-on-freedom-of-expression-online> (accessed on 22 May 2024).
34. How a Smart Home Works in Russia after Sanctions. Lots of Restrictions. Available online: <https://www.iphones.ru/iNotes/ka-k-rabotaet-umnyy-dom-v-rossii-posle-sankciy-08-09-2022> (accessed on 22 May 2024).
35. BMP280 Datasheet (PDF)—Bosch Sensortec GmbH. Available online: <https://www.alldatasheet.com/datasheet-pdf/pdf/1132069/BOSCH/BMP280.html> (accessed on 30 May 2024).
36. Madeti, S.R.; Singh, S.N. Monitoring System for Photovoltaic Plants: A Review. *Renew. Sustain. Energy Rev.* **2017**, *67*, 1180–1207. [\[CrossRef\]](#)
37. Sensors and Microcontrollers. Available online: <https://habr.com/ru/post/260639/> (accessed on 25 May 2024).
38. SOT23 INA219 Bi-Directional DC Current Power Supply Sensor Breakout Module Original DIY 3V-5V IIC I2C Power Monitoring Sensor. Available online: https://aliexpress.ru/item/1005003041425999.html?spm=a2g2w.orderdetail.0.0.4b3b4aa6Zk74w0&sku_id=12000023402820342 (accessed on 25 May 2024).
39. INA219 Datasheet (PDF)—Texas Instruments. Available online: <https://www.alldatasheet.com/datasheet-pdf/pdf/249609/TI/INA219.html> (accessed on 25 May 2024).
40. 8-Bit Microcontroller with 2/4K Bytes In-System Programmable Flash. Available online: <https://www.keysemi.com/upload/datasheet/attiny2313a-pu.pdf> (accessed on 25 May 2024).
41. TSOP31236 Datasheet (PDF)—Vishay Siliconix. Available online: <https://www.alldatasheet.com/datasheet-pdf/pdf/252281/VI/SHAY/TSOP31236.html> (accessed on 25 May 2024).
42. JDY-40-Datasheet. Available online: <https://www.rcscomponents.com/datasheets/JDY-40-datasheet.pdf> (accessed on 25 May 2024).

43. NI-ZN BATTERY SPECIFICATION. Available online: https://docviewer.yandex.kz/view/0/?page=1&*=hin5imxayp61e9MN43T2Rlw2XVd7InVybCI6Imh0dHA6Ly93d3cuZmlsbXB2Nlc3MucnUvaW1hZ2VzL290aGVycy9peGJ0L25pem4vY29ucmFkXzI1MDAucGRmliwidGl0bGUiOiJjb25yYWRfMjUwMC5wZGYiLCJub2lmcmFtZSI6dHJ1ZSwidWlkIjoiMCIsInRzIjoxNzE2ODY4NjE4MTYxLCJ5dSI6IjgzMjc2ODU5MzE2NzY5OTA2NTciLCJzZXJwUGFyYW1zIjoidG09MTcxNjg2ODYxMiZ0bGQ9a3oMbGFuZz1lbiZuYW1lPWNvbnJhZlF8yNTAwLnBkZiZ0ZXh0PU5JLVpOKzI1MDArbVdIKyVEMCVVCNCVEMCVCMCVEMSU4MiVEMCVCMCVEMSU4OCVEMCVCOCVEMSU4MiZ1cmw9aHR0cCUzQS8vd3d3LmZpbG1wcm9jZXNzLnJlL2ltYWdscy9vdGhlcnMvaXhidC9uaXpuL2NvbnJhZlF8yNTAwLnBkZiZscj0xOTAmbWltZT1wZGYmbDEwbj1ydSZzaWduPWYyMTIhNjliZmYwMTc5N2E3YmVmNDlhYmVjNzg3ZWZ3MjtleW5vPTAifQ==&lang=en (accessed on 28 May 2024).
44. Manukovsky, A.V.; Sagyndyk, A.B.; Talipov, O.M. Development of an Interference-Resistant Radio Channel to Organize Monitoring of the Operation of the «green Energy» Power Plant. *Bull. Toraighyrov Univ. Energetics Ser.* **2023**, 184–196. [[CrossRef](#)]
45. Kletsel, M.Y.A.; Alishev, Z.H.R.; Musin, V.V.; Manukovskij, A.V. Properties of reed switches used in relay protection. *Elektrichestvo* **1993**, 9, 18–21.

Disclaimer/Publisher’s Note: The statements, opinions and data contained in all publications are solely those of the individual author(s) and contributor(s) and not of MDPI and/or the editor(s). MDPI and/or the editor(s) disclaim responsibility for any injury to people or property resulting from any ideas, methods, instructions or products referred to in the content.